Bong Jae Lee[1]
Department of Mechanical Engineering,
Korea Advanced Institute of Science
and Technology,
Daejeon 305-701, South Korea
e-mail: bongjae.lee@kaist.ac.kr

Keunhan Park[1]
e-mail: kpark@egr.uri.edu

Timothy Walsh
Department of Mechanical,
Industrial and Systems Engineering,
University of Rhode Island,
Kingston, RI 02881

Lina Xu
Department of Mechanical Engineering and
Materials Science,
University of Pittsburgh,
Pittsburgh, PA 15261

Radiative Heat Transfer Analysis in Plasmonic Nanofluids for Direct Solar Thermal Absorption

The present study reports a novel concept of a direct solar thermal collector that harnesses the localized surface plasmon of metallic nanoparticles suspended in water. At the plasmon resonance frequency, the absorption and scattering from the nanoparticle can be greatly enhanced via the coupling of the incident radiation with the collective motion of electrons in metal. However, the surface plasmon induces strong absorption with a sharp peak due to its resonant nature, which is not desirable for broad-band solar absorption. In order to achieve the broad-band absorption, we propose a direct solar thermal collector that has four types of gold-nanoshell particles blended in the aquatic solution. Numerical simulations based on the Monte Carlo algorithm and finite element analysis have shown that the use of blended plasmonic nanofluids can significantly enhance the solar collector efficiency with an extremely low particle concentration (e.g., approximately 70% for a 0.05% particle volume fraction). The low particle concentration ensures that nanoparticles do not significantly alter the flow characteristics of nanofluids inside the solar collector. The results obtained from this study will facilitate the development of highly efficient solar thermal collectors using plasmonic nanofluids.
[DOI: 10.1115/1.4005756]

1 Introduction

A large number of studies have dealt with solar thermal collectors that utilize the solar radiation to generate the thermal energy [1–5]. One of the most common types of solar thermal collectors is a flat-plate collector [4] that collects the solar energy with a highly absorbing surface to heat the working fluid flowing in the collector. Due to the heat loss during the surface-induced solar absorption and heat transfer to the working fluid, the flat-surface collector cannot be used for high heat flux (or high temperature) environments, such as in concentrated solar collectors [2]. In order to minimize the heat loss at high temperatures, the black-liquid collector was proposed in the 1970s [1]. Since the solar energy is directly absorbed by the working fluid flowing in the transparent channel of the black-liquid collector, undesired heating of other collector components and the resultant loss of efficiency can be prevented [3]. However, the poor light-absorption characteristics of typical working fluids, such as pure water [6], in the visible spectrum inherently limits the performance of the black-liquid collector, suggesting that highly absorptive substances should be added to the working fluid to enhance the light absorption.

Recently, nanofluids (i.e., suspension of nanoparticles in a base fluid) have been used as a working fluid in the solar thermal collector to enhance the light-absorption characteristics [7–10]. For instance, aluminum nanoparticles suspended in water can improve the efficiency of a solar collector by about 10% [8] better than when using pure water. In addition, Sani et al. [9] demonstrated that single-wall carbon nanohorns play a significant role in improving the optical and thermal properties of the fluid. It is important to understand that the efficiency improvement of the nanofluid-based solar collector is primarily owing to the enhanced light absorption by nanoparticles in the working fluid. Thus, intrinsic optical properties of nanoparticles and their volume concentration are two key parameters in tuning the light-absorption characteristics of the resulting nanofluid.

It is well known that metallic nanoparticles can support localized surface plasmons at a certain frequency [11]. Surface plasmons are collective oscillations of the charge density at the interface between a metal and a dielectric medium [12]. When the surface plasmon is excited in metallic nanoparticles, the incident photon energy is resonantly transferred to the plasmon, resulting in a sharp increase of the light absorption. Therefore, the localized surface plasmon supported by metallic nanoparticles has great potential to improve the performance of direct solar thermal collection. However, there are two challenges in using the surface plasmon for solar thermal absorption. The first challenge lies in the sharp absorption peak of the surface plasmon, which does not meet the need for broad-band solar absorption. Moreover, the surface plasmon resonance frequency of metallic nanoparticles, such as gold, silver, and aluminum, is usually located in the ultraviolet to short visible range. Although intensive studies have been conducted on the applications of the surface plasmon for photovoltaics [13–16], the surface plasmon has not been explored for the solar thermal absorption.

The present paper proposes a nanofluid-based solar collection that makes use of the localized surface plasmon to enhance broad-band solar thermal absorption. In order to induce plasmon resonance across a broad-range solar spectrum from the visible to the near-infrared range, gold-nanoshell (GNS) nanoparticles with different SiO_2 core sizes and Au coating thicknesses are mixed in water to make a GNS-blended nanofluid. A Monte Carlo algorithm combined with the Mie scattering theory is developed to determine the absorption and scattering coefficients of the nanofluid and statistically calculate the solar thermal absorption across the collector channel by solving the radiative transfer equation. A finite element analysis is then implemented to calculate the temperature increase of the nanofluid and the resultant collector efficiency for a given Reynolds number. The subsequent chapters will describe the basic theory in modeling optical and thermal behaviors of the GNS-blended nanofluid, followed by the performance analysis of the proposed solar thermal collector in comparison with the existing designs.

2 Theoretical Modeling

As briefly discussed in the Introduction, the key to enhancing light absorption of nanofluid-based solar thermal collectors is the

[1]Corresponding authors.

Contributed by the Solar Energy Division of ASME for publication in the JOURNAL OF SOLAR ENERGY ENGINEERING. Manuscript received March 10, 2011; final manuscript received December 15, 2011; published online March 1, 2012. Assoc. Editor: Robert Palumbo.

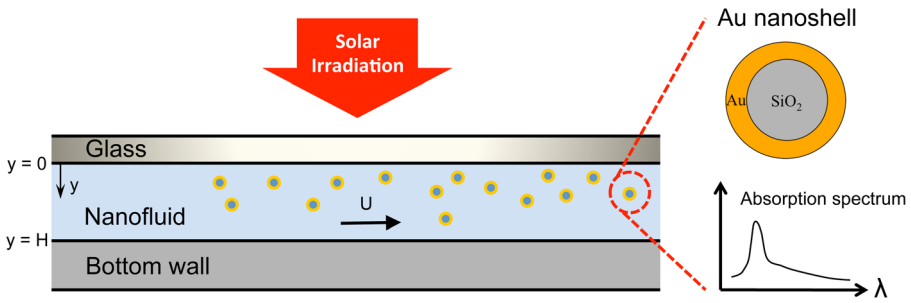

Fig. 1 Schematic of a nanofluid-based solar collector. Inset shows the schematic of the Au nanoshell and its absorption spectrum. Absorption peak occurs by the coupling with the localized surface plasmon.

excitation of the surface plasmon in the visible and near-infrared spectra. However, surface plasmon excitations of nanoparticles in the Rayleigh scattering regime are predetermined by the dielectric function of the particle ε_p as $\Re(\varepsilon_p) = -2\varepsilon_m$ [11], where ε_m is the dielectric function of the surrounding medium and $\Re$ takes the real part of a complex quantity, restricting the surface plasmon resonance to ultraviolet-visible region. This challenge can be overcome by employing core-shell-type nanoparticles. The inset of Fig. 1 illustrates a GNS particle used in this study, which is made of a SiO_2 core with an Au coating. Surface plasmons at both boundaries of the Au shell of the GNS particle interact with each other and separate the surface-plasmon dispersion curve into two branches, i.e., symmetric and asymmetric modes [17]. Due to this hybridization of plasmon excitation, the plasmon resonance frequency can be precisely tuned by adjusting the Au layer thickness, which allows one to control the absorption peak of the GNS nanofluid to match with the incident solar spectrum. Furthermore, in order to utilize the plasmon resonance in a broad spectral range, four types of GNSs with different SiO_2 core sizes and Au coating thicknesses are mixed with water to generate the GNS-blended nanofluid.

Figure 1 illustrates the schematic of the nanofluid-based solar collector where the GNS-blended nanofluid flows in a narrow channel with height H. The glass plate with the transmittance value of 90% [5] is used as the top cover to minimize evaporation of the fluid to the environment. It should be emphasized that when plasmonic nanoparticles are involved scattering cannot be neglected as previously done in Refs. [8] and [10], because the localized surface plasmon significantly enhances both scattering and absorption [18]. Therefore, complicated scattering phenomena should be fully taken into consideration.

In the present study, a Monte Carlo algorithm [19,20] was employed to solve the radiative transport equation (RTE) [21] with consideration of the volume scattering from nanoparticles in the nanofluid. At the same time, it was assumed that the volume scattering can be regarded as series of a single particle scattering (i.e., dependent scattering does not occur). This assumption can be justified when the particle volume fraction is very low, i.e., less than approximately 0.6%, with small particle size parameter, i.e., $\pi D/\lambda < 1$, where D is a particle diameter and λ is a wavelength of the incident light in vacuum [22]. In solving the RTE, absorption and scattering coefficients of the nanofluid blended with four types of GNSs are obtained from the absorption efficiency Q_{abs} and scattering efficiency Q_{scat} of each GNS and its volume fraction using [11]

$$\alpha_\lambda = \left(1 - \sum_{i=1}^{4} f_i\right)\alpha_{w,\lambda} + \sum_{i=1}^{4} \frac{3f_i}{2D_i} Q_{abs,i} \tag{1}$$

$$\sigma_\lambda = \sum_{i=1}^{4} \frac{3f_i}{2D_i} Q_{scat,i} \tag{2}$$

where $\alpha_{w,\lambda}$ is the absorption coefficient of water and f is the volume fraction of the individual GNS. The calculated absorption and scattering coefficients of the GNS-blended nanofluid will be discussed in Sec. 3.

In the Monte Carlo simulation, the drift process (during which the photon bundle propagates) is treated independently from the scattering process (during which the photon bundle changes its propagation direction) [23]. It is assumed that the drift process is followed by the scattering process based on the scattering probability $P_{\text{scat}} = 1 - \exp(-L\sigma_\lambda)$, where L is the propagation length of phonon bundle calculated by $L = -\ln(R_1)/(\sigma_\lambda + \alpha_\lambda)$. A uniform random number R_1 is generated to satisfy $0 \le R_1 \le 1$ by the quasi-random sequence [24]. Notice that the estimated L stochastically represents the mean-free-path (i.e., averaged propagation length) of $1/(\sigma_\lambda + \alpha_\lambda)$. In order to determine whether to accept or reject the scattering event, another uniform random number R_2 is generated and compared with P_{scat}; if $R_2 \le P_{\text{scat}}$, the ray will be scattered upon encountering a nanoparticle. Upon the scattering process, the postscattering direction of the photon bundle is described by the polar angle and the azimuth angle with respect to the prescattering direction vector. For the simplicity, the polar angle is stochastically determined by transforming the Henyey–Greenstein (H–G) scattering phase function [25], and the azimuthal angle is determined by assuming that the scattering is isotropic in the azimuthal direction. It should be noted that the H–G scattering phase function is an approximation and cannot be regarded as the rigorous phase function for the light scattering from the GNS. Nevertheless, H–G scattering phase function provides the probability density of light scattering that can be seamlessly integrated to the Monte Carlo simulation without losing consistency.

Although the absorption of the GNS-blended nanofluid is mainly due to the plasmonic absorption by nanoparticles, the Monte Carlo simulation treats the nanofluid as an effective medium, in which the energy of the photon bundle uniformly reduces by a factor of $e^{-\alpha_\lambda L}$ due to volumetric absorption while traveling a distance L. When the photon bundle reaches the bottom surface (i.e., at $y = H$), there is no reflection back into the medium. However, when the photon bundle is back-scattered to the top cover (i.e., at $y = 0$), it is reflected back to the medium with a 47% probability, which is based on the hemispherical reflectance at the top surface (i.e., water–glass–air interfaces). The drift and scattering processes will be repeated until the photon bundle leaves the channel or 99.9% of its energy is absorbed inside the nanofluid.

The most important quantities to be estimated from the Monte Carlo simulation is the volumetric solar energy absorption rate in the nanofluid. In the simulation, the spectral solar irradiation normally incident on the solar collector can be approximated as $G_\lambda(\lambda) = I_{b,\lambda}(\lambda, T_s)\Omega_s$, where $\Omega_s = 6.80 \times 10^{-5}$ sr is the solid angle of the sun from the earth, and $I_{b,\lambda}$ is the spectral intensity of the sun, which is the blackbody intensity at the temperature of the sun, $T_s = 5777$ K [22]. By tracing each photon bundle undergoing scattering processes and calculating the energy absorption during drift processes, the Monte Carlo simulation can provide the spectral absorptance distribution across the collector channel depth,

$A_\lambda(\lambda, y)$. The volumetric solar energy absorption rate can then be written as

$$\dot{q}_{tot}(y) = \frac{d}{dy}\int_{\lambda_{min}}^{\lambda_{max}} \tau_g A_\lambda(\lambda, y) G_\lambda(\lambda) d\lambda \tag{3}$$

where τ_g is the transmittance of the top glass cover. For the calculation, we set $\lambda_{\min} = 200$ nm and $\lambda_{\max} = 2000$ nm.

In order to predict the temperature profile within the nanofluid under solar absorption, momentum and energy balances are conducted based on the steady-state, two-dimensional (2D) approximation. Under laminar flow conditions with no body force, the Navier–Stokes and heat transport equations are numerically solved using a COMSOL Multiphysics commercial package. Since the volume fraction of plasmonic nanoparticles is very low (i.e., less than 1%), thermophysical properties of the GNS-blended nanofluid, such as density ρ, specific heat c_p, thermal conductivity k, and dynamic viscosity μ, are assumed to be the same as those of pure water [26]. The 2D collector geometry selected for the computation is $L_c = 1$ m for the channel length, $H = 1.5$ mm for the channel height, and $t_g = 1$ mm for the glass cover thickness. These geometric parameters were intentionally chosen to be similar with values in Ref. [8] for comparison purpose. Boundary conditions for the heat transport equation are set to be $T(0, y) = T_{in}$, $k\frac{\partial T}{\partial y}|_{y=-t_g} = h[T(x, -t_g) - T_\infty]$, and $\frac{\partial T}{\partial y}|_{y=H} = 0$. Here, $T_{in} = 293.15$ K is the uniform inlet temperature of the nanofluid, $h = 10$ W/m^2 K is the convection heat transfer coefficient at the top surface, and $T_\infty = 293.15$ K is the ambient temperature. As for the Navier–Stokes equation, the inlet velocity is set to be uniform in x-direction. For the numerical simulation, 10,848 triangular mesh elements were made in the collector domain shown in Fig. 1 as a schematic. In order to avoid mesh-dependence of the solution and increases the computational speed, the meshes were made with a 5:1 scale factor in the y-direction. Temperature dependence of the thermophysical properties was also considered in the computation.

Finally, the collector efficiency is estimated by [8]

$$\eta = \frac{\dot{m} c_p (\bar{T}_{out} - T_{in})}{A G_T} \tag{4}$$

where $\dot{m}$ is the mass flow rate, $\bar{T}_{out}$ is the mean outlet temperature, A is the top cover area of the collector, and G_T is the incident solar flux given by $G_T = \int_{\lambda_{min}}^{\lambda_{max}} G_\lambda d\lambda$. The above equation results in $G_T = 1367$ W/m^2, which is essentially the same as the solar constant [2]. Since Eq. (3) does not account for the scattering and absorption by the atmosphere, the solar constant was used as the incident solar flux for consistency.

3 Results and Discussion

The absorption efficiency Q_{abs} and the scattering efficiency Q_{scat} of the individual GNS can be expressed based on the Mie scattering coefficients of the core-shell nanoparticle as [11]

$$Q_{scat} = \frac{2}{x^2}\sum_{n=1}^{\infty}(2n+1)(|a_n|^2 + |b_n|^2) \tag{5}$$

$$Q_{abs} = \frac{2}{x^2}\sum_{n=1}^{\infty}(2n+1)\Re(a_n + b_n) - Q_{\text{scat}} \tag{6}$$

where size parameter x is given by $x = (2\pi n_w r_o)/\lambda$ with the refractive index of water (n_w), and the outer radius of core-shell (r_o). Here, the Mie scattering coefficients a_n and b_n for the core-shell structure are calculated in a similar way to Airy's formulae for the multilayer thin films by considering the interference between forwardly and backwardly propagating spherical waves [27]. Notice that in nanoparticles with sizes much smaller than the mean-free-path of the conduction electrons, the optical properties may be modified, which leads to broadening of the plasmonic effects. The size-dependent dielectric function of Au is calculated by using the Drude model with modified scattering rate as [10,28]

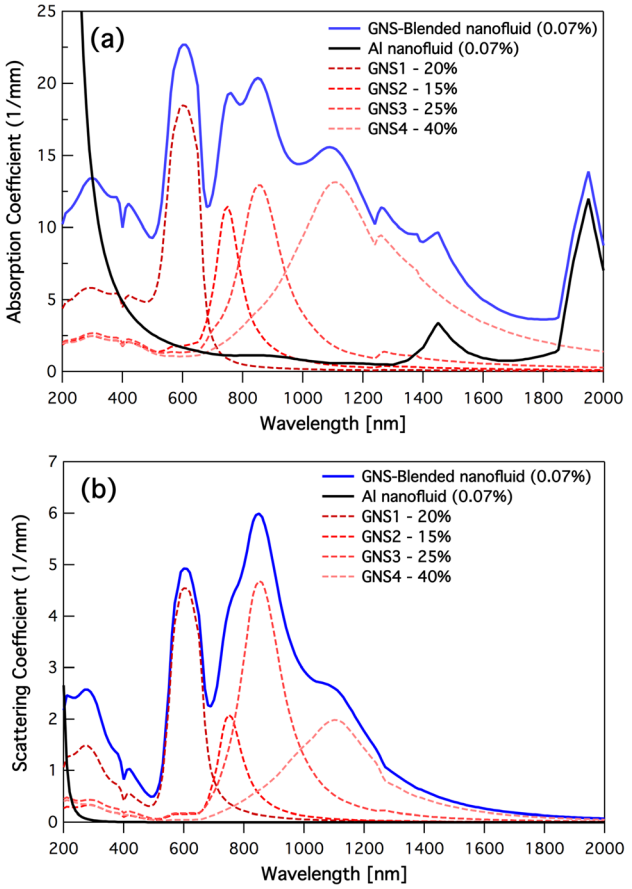

Fig. 2 Absorption (*a*) and scattering (*b*) coefficients of the GNS-blended nanofluid. Each GNS's contributions to the overall absorption and scattering coefficients are denoted by dashed line. For comparison purpose, absorption and scattering coefficients of the Al ($r = 2.5$ nm) nanofluid are also plotted.

$$\varepsilon(\omega) = \varepsilon_{bulk}(\omega) + \omega_p^2\left(\frac{1}{\omega^2 + \Gamma_\infty^2} - \frac{1}{\omega^2 + \Gamma^2}\right) + i\frac{\omega_p^2}{\omega}\left(\frac{\Gamma}{\omega^2 + \Gamma^2} - \frac{\Gamma_\infty}{\omega^2 + \Gamma_\infty^2}\right) \tag{7}$$

where ω_p is the plasma frequency and Γ_∞ is the scattering rate of bulk Au. These values are obtained from Ref. [29] as $\omega_p = 7.28 \times 10^4$ cm^{-1} and $\Gamma_\infty = 215$ cm^{-1}. In the above equation, the scattering rate of thin Au film is related to the bulk value by $\Gamma = \Gamma_\infty + v_F/t_{\text{Au}}$ with v_F and t_{Au} being the Fermi velocity and thickness of Au film, respectively. The optical constants of bulk Au, SiO_2, and water were obtained from Ref. [30].

Figure 2 shows the absorption and scattering coefficients of the GNS-blended nanofluid that contains four types of GNS nanoparticles, whose geometric parameters and relative portions to the total volume fraction are summarized in Table 1. The total volume fraction was 0.07% for the calculation. For comparison, Fig. 2 also plots the absorption and scattering coefficients of the nanofluid with Al particles ($r = 2.5$ nm and volume fraction 0.07%) used in Ref. [8]. The size effect of the Al dielectric function has also been considered in a similar way to Au. The light absorption and scattering of the Al nanofluid are very strong at around

Table 1 Geometric parameters of four types of GNSs and their relative portion toward the total volume fraction

	SiO_2 core radius (nm)	Au thickness (nm)	relative portion (%)
GNS1	20	10	20
GNS2	30	5	15
GNS3	45	5	25
GNS4	55	3	40

200 nm due to the surface plasmon excitation of Al nanoparticles in the ultraviolet region. However, in most visible and near-infrared spectra that are important for the solar absorption, GNS-blended nanofluid exhibits the superior absorption performance than the Al nanofluid at the same volume fraction. As can be seen from Fig. 2 (refer to dashed lines), the wavelength corresponding to the absorption peak of individual GNS can be tuned by changing the geometric parameters of core-shell nanoparticle (i.e., 610 nm for GNS1, 750 nm for GNS2, 860 nm for GNS3, and 1110 nm for GNS4,). This tunability of the surface plasmon excitation is the great advantage of engineering GNS nanoparticles for the effective solar thermal absorption. It is also worthwhile to note that the thin Au coating thickness less than the mean-free-path of free electrons is actually beneficial to achieve the broad-band absorption peak (see GNS4). As mentioned earlier, the scattering effect should be carefully considered for the GNS-blended nanofluid, differently from the previous work using Al nanofluid [8] that ignored the in-scattering term in the RTE due to the low scattering coefficient over the spectrum of interest. To this end, Monte Carlo simulation was implemented in this study.

The spectral solar irradiation is plotted in Fig. 3 at different depths in the solar collector when the channel height $H = 1.5$ mm. As indicated with dotted lines at four different wavelengths, the localized surface plasmons on the GNS significantly contribute to the spectral solar absorption, showing that more than 95% of the solar irradiation is absorbed through $y = 0.5\ H$. At this point, the solar irradiation becomes nearly uniform with a small value (i.e., < 200 W/m^2 μm). The inset of Fig. 3 shows the volumetric heat generation rate given in Eq. (3). The absorption of solar irradiation occurs mostly near the top glass surface (i.e., $y < 0.2\ H$), indicating that increasing the channel height may not improve the overall efficiency of the solar collector unless the concentrating collector design is used.

The efficiency of the solar collector based on the GNS-blended nanofluid is plotted in Fig. 4. In the calculation, the composition of the four types of GNSs is fixed as listed in Table 1 while the total volume fraction varies. The Reynolds number for the

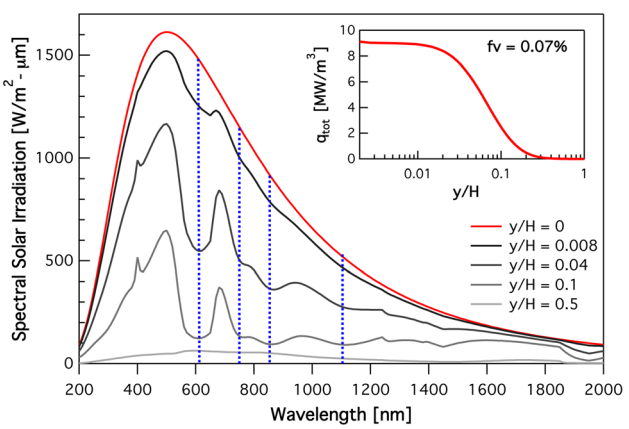

Fig. 3 Spectral solar irradiation versus the wavelength at various depths in the solar collector with the GNS-blended nanofluid at the total volume fraction 0.07%. The inset shows the volumetric heat generation at different locations in the solar collector.

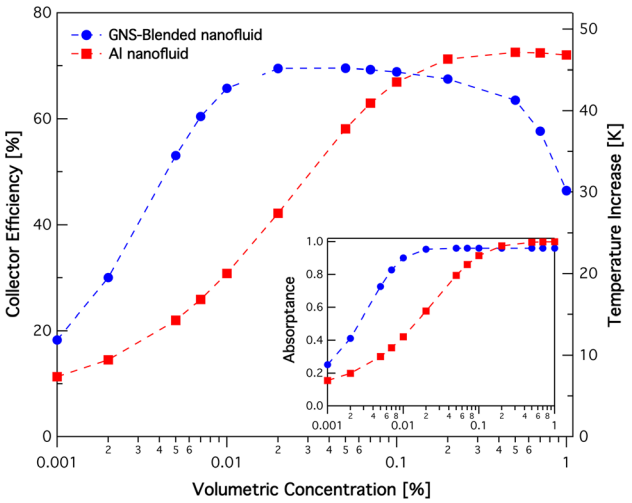

Fig. 4 Predicted efficiency of the solar collector with the GNS-blended nanofluid (circular symbol) or the Al ($r = 2.5$ nm) nanofluid (square symbol) versus the volume fraction at $Re_H = 10$. For the GNS-blended nanofluid, the volume fraction means the total volume concentration of four types of GNSs. The inset shows the total absorptance in the solar collector as a function of the volume fraction.

calculation was set to $Re_H = \rho U_{in} H/\mu = 10$, corresponding to the inlet velocity $U_{in} = 0.0033$ m/s. From the figure, it is clear that the volume fraction of GNS nanoparticles plays a critical role in the collector efficiency. As the volume fraction increases, the collector efficiency increases to reach the maximum value of approximately 70% in the 0.02–0.1% volume fraction range and starts decreasing as the GNS concentration further increases. As a result, the temperature increase (i.e., $\bar{T}_{out} - T_{in}$) reaches as high as 45 K at the maximum collector efficiency as indicated by the secondary y-axis of the figure. The efficiency increase in the small concentration regime is due to the high absorption induced by the surface plasmon excitation on each GNS nanoparticle. However, when the GNS volume fraction exceeds 0.1%, more energy is absorbed in the vicinity of the top glass cover, and thus more heat will be lost to the air instead of being transferred to the nanofluid. The inset of Fig. 4 is also consistent with this reasoning such that the total amount of the absorbed solar energy is nearly the same when the GNS volume fraction is greater than 0.1% although the collector efficiency starts to quickly decrease when the volume fraction is greater than 0.5%.

Figure 4 also exhibits the collector efficiency when the Al ($r = 2.5$ nm) nanofluid is used. The collector efficiency for the Al nanofluid reaches a maximum of about 70% near the volume concentration of 0.7%. This value is almost 10% lower than the efficiency predicted in Ref. [8] for the same particle and concentration. The discrepancy in the estimated efficiency may come from the fact that Ref. [8] used an incident solar flux of 1000 W/m^2, not the solar constant (i.e., $G_T = 1367$ W/m^2) for the efficiency calculation. Although this reduced solar flux reflects the atmospheric absorption and scattering, the atmospheric effect was not consistently considered in the calculation of the radiative transfer equation in Ref. [8]. As shown in the figure, the collector efficiency of the GNS-blended nanofluid is comparable to that of the Al nanofluid although the volume concentration is one order of magnitude lower. This is a great advantage of employing plasmonic nanofluids for the solar thermal absorption.

In order to provide more detailed information about the effects of the GNS concentration on the solar thermal absorption, Fig. 5 compares the normalized volumetric solar energy absorption rates and corresponding temperature distributions within the solar collector for different GNS volume fractions. For the normalization, maximum $\dot{q}_{tot}$ and temperature at each concentration were

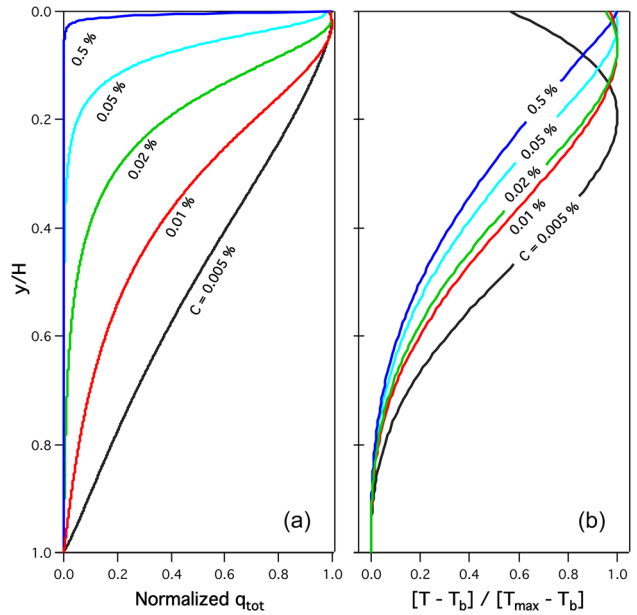

Fig. 5 (*a*) Volumetric heat generation rates and (*b*) corresponding temperature distributions within the solar collector for different GNS concentrations. The plot is normalized for clear comparison. Note that T_b stands for the temperature at the bottom wall surface (i.e., $y = H$).

implemented to plot $\dot{q}_{tot}(y)/\dot{q}_{tot,max}$ and $[T(y) - T_b]/[T_{\max} - T_b]$, where T_b is the temperature at the channel bottom, $y = H$. Figure 5(*a*) reveals that the maximum of the volumetric heat generation appears at slightly below the top glass cover: see 0.01% case, for instance. This is due to the back scattering of photon bundles near the top glass cover. Since the nanofluid with a lower particle concentration has a larger radiation penetration depth, the solar energy propagates deeper into the channel before absorption, resulting in more uniform heat generation and more parabolic temperature distribution across the channel as shown in Fig. 5(*b*). However, as the concentration increases, the radiation penetration depth of the nanofluid becomes smaller, confining the solar energy absorption in the vicinity of the top surface, $y = 0$. This thin absorption layer at a high concentration locates the maximum temperature point to the top surface and causes the temperature to monotonically decrease toward the bottom surface. It should be noted that heat transfer in the y-direction of the channel is only by conduction in the laminar flow regime. Thus, the nanoparticle concentration is critically important not only for the collector efficiency but also for the uniformity of the resultant temperature distribution.

The inlet flow velocity is another important factor that significantly influences the performance of the solar thermal collector. Figure 6 shows the collector efficiency and the average temperature increase across the 1-m-long channel as a function of the Reynolds number. As defined in Eq. (4), the collector efficiency is determined by the amount of energy carried by the nanofluid flow, i.e., $\dot{m}c_p(\bar{T}_{out} - T_{in})$. Thus, the heat loss to the environment should be minimized for a higher collector efficiency. As the inlet velocity (or Re_H) increases, the nanofluid flows faster in the channel while losing less heat to the environment via convection, making a positive effect on the collector efficiency. However, the nanofluid has less time to be heated by solar absorption, decreasing the outlet temperature. These opposite trends are well observed in Fig. 6, suggesting that the geometric parameters and operating conditions of the solar thermal collector should be carefully designed according to the needs of a specific application. For example, the channel length could be elongated to achieve a large temperature increase for a high Reynolds number, but it will adversely affect the collector efficiency. Likewise, the solar concentration is crucial for the high throughput of solar thermal conversion, but it may compromise the collector efficiency due to the increase in the heat loss to the environment. The optimization of design parameters for the best performance of the proposed solar collector will be left as future experimental research.

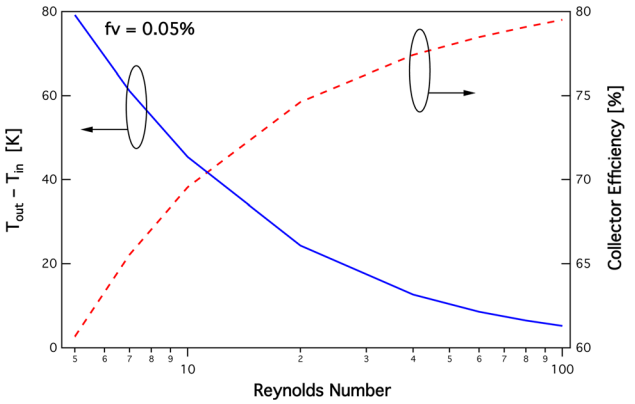

Fig. 6 Effect of Reynolds number on the average temperature increases across the channel and the corresponding collector efficiency

4 Conclusions

The present paper has theoretically investigated the performance of a direct solar thermal collector that employs plasmonic nanoparticles suspended in water. In order to broaden the sharp absorption peak associated with the surface plasmon, the GNS-blended nanofluid, i.e., four types of GNSs with different SiO_2 core sizes and Au layer thicknesses suspended in water, has been proposed as a conceptual design. Since the light scattering cannot be neglected for the plasmonic nanofluid, the present study has developed a Monte Carlo scheme to statistically solve the radiative transfer equation by fully considering the in- and out-scattering term. Numerical simulations using the Monte Carlo method and the finite element analysis have demonstrated that the use of the GNS-blended nanofluid can significantly enhance the solar collector efficiency even at an extremely low particle concentration (e.g., approximately 70% efficiency with 0.05% particle volume fraction), which is at least 1 order of magnitude lower than the current technology. Parametric studies also reveal that the particle concentration influences the uniformity of the solar energy absorption and associated temperature distribution at the outlet. However, the average temperature increases across the 1-m-long channel is about 45 K at the maximum collector efficiency and even smaller for a high Reynolds number, strongly suggesting that a concentrating collector design may be necessary for real world applications where the solar thermal collector is coupled to the power generating cycle. Optimization of geometries and operation conditions are highly necessary to achieve the high collector efficiency and large temperature increase in the solar thermal energy conversion.

Acknowledgment

This work was mainly supported by the National Science Foundation (CBET-0966868 through PITT and CBET-1067441 through URI). B.J.L. thanks for the partial support from the startup program at KAIST, and K.P. also appreciates the partial support from the RI/Brown RI Consortium for Nanoscience and Nanotechnology.

Nomenclature

A = area (m^2)
c_p = specific heat (kJ/kg K)
D = diameter (m)

f = volume fraction
H = height (m)
h = convection heat transfer coefficient (W/m^2 K)
I = intensity (W/m^2 sr μm)
k = thermal conductivity (W/m K)
L = length (m)
$\dot{m}$ = mass flow rate (kg/s)
P = probability
Q = absorption (or scattering) efficiency
$\dot{q}$ = volumetric heat generation rate (W/m^3)
R = uniform random number
r = radius (m)
t = thickness (m)
U = flow velocity (m/s)

Greek Symbols

α = absorption coefficient (1/m)
ε = dielectric function
η = collector efficiency (%)
λ = wavelength in vacuum (m)
μ = viscosity (kg/s m)
σ = scattering coefficient (1/m)
τ = transmittance
Ω = solid angle (sr)

Subscripts

abs = absorption
c = channel
in = inlet
g = glass
out = outlet
s = sun
scat = scattering
tot = total
w = water
λ = spectral

References

[1] Minardi, J. E., and Chuang, H. N., 1975, "Performance of a 'Black' Liquid Flat-Plate Solar Collector," Sol. Energy, **17**, pp. 179–183.
[2] Duffie, J. A., and Beckman, W. A., 1980, *Solar Thermal Engineering Processes*, Wiley, New York.
[3] Sodha, M., Bansal, N. K., and Singh, D., 1984, "Analysis of a Black Liquid Flat Plate Solar Collector," Int. J. Energy Res., **8**, pp. 31–37.
[4] Okujagu, C. U., and Adjepong, S. K., 1989, "Performance of a Simple Flat Plate Solar Collector at an Equatorial Location," Sol. Wind Technol., **6**, pp. 283–289.
[5] Kalogirou, S. A., 2004, "Solar Thermal Collectors and Applications," Prog. Energy Combust. Sci., **30**, pp. 231–295.
[6] Otanicar, T. P., Phelan, P. E., and Golden, J. S., 2009, "Optical Properties of Liquids for Direct Absorption Solar Thermal Energy Systems," Sol. Energy, **83**(7), pp. 969–977.
[7] Kumar, S., and Tien, C. L., 1990, "Analysis of Combined Radiation and Convection in a Particulate-Laden Liquid Film," ASME J. Sol. Energy Eng., **112**(4), pp. 293–300.
[8] Tyagi, H., Phelan, P., and Prasher, R., 2009, "Predicted Efficiency of a Low-Temperature Nanofluid-Based Direct Absorption Solar Collector," ASME J. Sol. Energy Eng., **131**, p. 041004.
[9] Sani, E., Barison, S., Pagura, C., Mercatelli, L., Sansoni, P., Fontani, D., Jafrancesco, D., and Francini, F., 2010, "Carbon Nanohorns-Based Nanofluids as Direct Sunlight Absorbers," Opt. Express, **18**, pp. 5179–5187.
[10] Otanicar, T. P., Phelan, P. E., Prasher, R. S., Rosengarten, G., and Taylor, R. A., 2010, "Nanofluid-Based Direct Absorption Solar Collector," J. Renewable Sustainable Energy, **2**(3), p. 033102.
[11] Bohren, C. F., and Huffman, D. R., 1983, *Absorption and Scattering of Light by Small Particles*, Wiley, New York.
[12] Raether, H., 1988, *Surface Plasmons on Smooth and Rough Surfaces and on Gratings*, Springer-Verlag, Berlin, Germany.
[13] Derkacs, D., Lim, S., Matheu, P., Mar, W., and Yu, E. T., 2006, "Improved Performance of Amorphous Silicon Solar Cells via Scattering From Surface Plasmon Polaritons in Nearby Metallic Nanopar-Ticles," Appl. Phys. Lett., **89**, 093103.
[14] Temple, T. L., Mahanama, G. D. K., Reehal, H. S., and Bagnall, D. M., 2009, "Influence of Localized Surface Plasmon Excitation in Silver Nanoparticles on the Performance of Silicon Solar Cells," Sol. Energy Mater. Sol. Cells, **93**(11), pp. 1978–1985.
[15] Atwater, H. A., and Polman, A., 2010, "Plasmonics for Improved Photovoltaic Devices," Nature Mater., **9**(3), pp. 205–213.
[16] Pillai, S., and Green, M. A., 2010, "Plasmonics for Photovoltaic Applications," Sol. Energy Mater. Sol. Cells, **94**(9), pp. 1481–1486.
[17] Prodan, E., Radloff, C., Halas, N. J., and Nordlander, P., 2003, "A Hybridization Model for the Plasmon Response of Complex Nanostructures," Science, **302**, pp. 419–422.
[18] Xu, L., Lee, B. J., Hanson, W. L., and Han, B., 2010, "Brownian Motion Induced Dynamic Near-Field Interaction Between Quantum Dots and Plasmonic Nanoparticles in Aqueous Medium," Appl. Phys. Lett., **96**, p. 174101.
[19] Howell, J. R., 1998, "The Monte Carlo Method in Radiative Heat Transfer," ASME J. Heat Transfer, **120**, pp. 547–560.
[20] Li, Q., Lee, B. J., Zhang, Z. M., and Allen, D. W., 2008, "Light Scattering of Semitransparent Sintered Polytetrafluoroethylene Films," J. Biomed. Opt., **13**, p. 054064.
[21] Siegel, R., and Howell, J. R., 2002, *Thermal Radiation Heat Transfer*, Taylor & Francis Group, New York.
[22] Modest, M. F., 2003, *Radiative Heat Transfer*, Academic Press, San Diego, CA.
[23] Lacroix, D., Joulain, K., and Lemonnier, D., 2005, "Monte Carlo Transient Phonon Transport in Silicon and Germanium at Nanoscales," Phys. Rev. B, **72**(6), p. 064305.
[24] Flannery, B. P., Press, W., Teukolsky, S., and Vetterling, W., 1992, *Numerical Recipes in C*, Press Syndicate of the University of Cambridge, New York.
[25] Wang, L., Jacques, S. L., and Zheng, L., 1995, "MCML-Monte Carlo Modeling of Light Transport in Multi-Layered Tissues," Comput. Methods Programs Biomed., **47**(2), pp. 131–146.
[26] Das, S., Choi, S., Yu, W., and Pradeep, T., 2008, *Nanofluids: Science and Technology*, Wiley-Interscience, Hoboken, NJ.
[27] Smith, D. D., and Fuller, K. A., 2002, "Photonic Bandgaps in Mie Scattering by Concentrically Stratified Spheres," J. Opt. Soc. Am. B, **19**(10), pp. 2449–2455.
[28] Nehl, C., Grady, N., Goodrich, G., Tam, F., Halas, N., and Hafner, J., 2004, "Scattering Spectra of Single Gold Nanoshells," Nano Lett., **4**(12), pp. 2355–2359.
[29] Ordal, M., Bell, R., Alexander, R., Jr., Long, L., and Querry, M., 1985, "Optical Properties of Fourteen Metals in the Infrared and Far Infrared: Al, Co, Cu, Au, Fe, Pb, Mo, Ni, Pd, Pt, Ag, Ti, V, and W," Appl. Opt., **24**(24), pp. 4493–4499.
[30] Palik, E. D., and Ghosh, G., 1998, *Handbook of Optical Constants of Solids: Five-Volume Set*, Academic, San Diego, CA.